Electrocatalytic properties of prussian blue nanoparticles supported on poly(*m*-aminobenzenesulfonic acid)–functionalized single-walled carbon nanotubes toward the detection of dopamine

Abolanle S. Adekunle[1,2*], Abdullahi M. Farah[3], Jeseelan Pillay[4], Kenneth I. Ozoemena[5,6], Bhekie B. Mamba[2] and Bolade O. Agboola[7*]

[1]*Department of Chemistry, Obafemi Awolowo University, Ile-Ife, Nigeria.*

[2]*Department of Chemical Technology, University of Johannesburg, P.O. Box 17011, Doornfontein, 2028, South Africa.*

[3]*Department of Chemistry, Vaal University of Technology, Johannesburg, South Africa.*

[4]*Advanced Materials Division, MINTEK, Randburg 2125, South Africa.*

[5]*Energy & Processes Unit, Materials Science and Manufacturing, Council for Scientific and Industrial Research (CSIR), Pretoria 0001, South Africa*

[6]*Department of Chemistry, University of Pretoria, Pretoria, South Africa*

[7]*Petroleum Chemistry and Engineering Department, American University of Nigeria, Yola, Nigeria.*

Manuscript to be submitted to Colloid and Surfaces B

*Corresponding Authors: E-mail address: bolade.agboola@aun.edu.ng, bolade_agboola@yahoo.co.uk, sadek2k@yahoo.com

Abstract

Edged plane pyrolytic graphite electrode (EPPGE) was modified with and without Prussian blue (PB) nanoparticles and polyaminobenzene sulphonated single-walled carbon nanotubes (SWCNTPABS) using the chemical deposition method. The electrodes were characterised using microscopy, spectroscopy and electrochemical techniques. Results showed that edged plane pyrolytic graphite-single-walled carbon nanotubes-prussian blue (EPPGE-SWCNT-PB) electrode gave the best dopamine (DA) current response which increases with increasing PB layers. The catalytic rate constant of 1.69×10^5 $mol^{-1}cm^3s^{-1}$, Tafel value of 112 $mVdec^{-1}$, and limit of detection of DA (2.8 nM) were obtained. Dopamine could be simultaneously detected with ascorbic acid. The electrode was found to be electrochemically stable, reusable and can be used for the analysis of DA in real drug samples.

Keywords: Prussian blue nanoparticles; Dopamine; Electrochemical impedance spectroscopy; Interferences; Ascorbic acid

1.0 Introduction

Carbon nanotubes (CNTs) are excellent electrical conducting nanowires with unique properties such as high tensile strength, electrical conductivity, chemical stability and flexibility. They are essential and promising materials in the field of nano-science and nanotechnology because of their electronic properties and large surface area [1-3]. Their contribution to the improvement of electrical properties of some bare electrode such as the glassy carbon [4-6], graphite [7-10], carbon fiber [11], gold [12-15], and platinum (Pt) electrodes [16] have been reported. As part of its numerous applications, Han et al. [17] considered CNTs as suitable mediators for prussian blue (PB)-modified electrodes because of their good electrical conductivity and the property of being particle carriers.

Prussian blue (PB) is a polynuclear and mixed-valent iron cyanide complex with a repeating unit of potassium ferrous ferricyanide hexacyano hexahydrate ($Fe_4(III)[Fe(II)(CN)_6]_3$). Prussian blue has unique properties in its structural arrangement which allows compositional variation by combining with several transition metal ions in different oxidation states such as Co^{2+}, and Co^{3+}, and Ni^{2+} [18]. This metal substitution and variation leads to a combination of properties that are not readily found in other inorganic materials [19]. Its unique properties, synthetic versatility and the ability of the cyanide ligands to bridge other ions have been explored in its application in electrochromic devices [20], nanomagnetic devices [21], biomedical sensor

[22], molecular sieves [23], catalysis [24] and in solid-state batteries [25]. Prussian blue nanoparticles exhibit excellent electrical properties which are different from those of their bulk. Among other methods, electrochemical deposition [26], chemical deposition [27] and the self-assembling method [23] have been used for PB decoration on electrodes. Agents, such as anionic surfactant sodium bis (2-ethylhexyl) sulfosuccinate [28], sodium hexametaphosphate [29], apoferritin [30], stearylamine [31] or nafion [32] are used to stabilize PB nanoparticles on electrode surfaces [33]. However, some of these binders may result in poor electrical conductivity of the electrode. PB prepared by chemical deposition was considered to be more stable within a wide range of pH [17] compared to the electrochemical method of preparation where PB properties can be affected by preparation conditions such as potential [26], current [34], and scan rate [26]. The self assembling method, on the other hand, results in polymolecules which increases the impedance of the electrode [17].

There have been reports on excellent interaction between CNTs and PB through $\pi-\pi$ interaction [35] and electrostatic attraction [36]. Carbon nanotubes Prussian blue (CNTs-PB) modified electrodes have been applied in the detection of many biomolecules including hydrogen peroxide [19,21], haemoglobin [37], glucose [27], and DNA [38]. Recently, there was a report on the electrocatalytic oxidation of diethylaminoethanethiol and hydrazine using SWCNT-PB modified electrode [39]. However, to the best of our

knowledge, there are no literature reports on the detection of dopamine using the edged plane pyrolytic graphite electrode-single-walled carbon nanotubes-prussian blue (EPPGE-SWCNT-PB) nanocomposite modified electrode.

Dopamine (DA) is a well known biomolecule that acts as a neurotransmitter in both the central and peripheral nervous system. Low concentration of this compound in the extra cellular fluid of the caudate nucleus or its complete depletion has been associated with Parkinson's disease in which causes the affected patient not to have the ability to control over his/her movement [40,41]. Other diseases resulting from abnormal metabolism of dopamine include epilepsy and senile dementia [42,43]. Thus, there is need for the fabrication of sensitive, specific and selective biosensors that would discriminately detect DA in the presence of other interfering species such as ascorbic and uric acids. This study explores the unique properties of SWCNT-PB nanocomposite formed *via* sequential chemo-synthetic steps on a pyrolytic graphite electrode. In this paper, we show that the fabrication of this electrode is simple and, more importantly, provides well-defined voltammograms for catalytic detection of dopamine, as well as simultaneous detection of dopamine in the presence of ascorbic acid. We also demonstrated the effect of the PB layers in EPPGE-SWCNT-PB electrodes on the DA current response.

2.0 Experimental

2.1 Materials and Reagents

Single-walled carbon nanotube-poly(*m*-aminobenzenesulfonic acid) (SWCNTPABS) was purchased from Aldrich Chemicals and was used directly without further treatment. $K_4[Fe(CN)_6].6H_2O$, dopamine-hydrochloride, cetyltrimethylammonium bromide (CTAB) were purchased from Sigma-Aldrich. Other chemicals and reagents were of analytical grade. Dopamine drug (Dopamine HCl-Fresenius® (200 mg / 5 ml) was supplied by a local pharmacy store. Ultra pure water of resistivity 18.2 MΩcm was obtained from a Milli-Q Water System (Millipore Corp., Bedford, MA, USA) and was used throughout for the preparation of solutions. A phosphate buffer solution (PBS) of pH 7.0 was prepared with appropriate amounts of $NaH_2PO_4.2H_2O$ and $Na_2HPO_4.2H_2O$, and the pH adjusted with 0.1 M H_3PO_4 or NaOH. All aqueous solutions prepared were purged with pure nitrogen to eliminate oxygen or any form of external oxidation during experiments. All electrochemical experiments were performed with nitrogen-saturated PBS.

2.2 Equipment and Procedure

The edge plane pyrolytic graphite electrode plate (3 mm diameter) was purchased from Le Carbone, Sussex, UK and was constructed locally at the University of Pretoria technical workshop. The plate was placed in a teflon tube, extended outside with a copper wire to make electrical contact with the

electrochemical equipment. The energy dispersive X-ray spectra were obtained from NORAN VANTAGE (USA). Atomic force microscopy (AFM) experiments were performed with AFM 5100 System (Agilent Technologies, USA) using a contact mode AFM scanner interfaced with a PicoView 1.4.3 controller (scan range 1.25 μm in x–y and 2.322 μm in z). Silicon type PPP-CONT-20 (Nanosensors®) of thickness 2.0±1.0 μm, length 450±10 μm, width 50±7.5 μm, spring constants 0.02-0.77 N m^{-1}, resonant frequencies of 6–21 kHz and tip height of 10-15 μm were used. All images (256 samples/line × 256 lines) were taken in air at room temperature at scan rates of 0.5–0.6 lines s^{-1}. UV/Vis experiment was performed with a UV-Visible spectrophotometer, 100 Bio Varian Win UV, Australia.

Electrochemical experiments were carried out using an Autolab Potentiostat PGSTAT 302 (Eco Chemie, Utrecht, and The Netherlands) driven by the GPES software version 4.9. Electrochemical impedance spectroscopy (EIS) measurements were performed with an Autolab Frequency Response Analyser (FRA) software between 10 kHz and 0.1 Hz using a 5 mV rms sinusoidal modulation with a solution of 0.1 M KCl in phosphate buffer solution of pH 7.0 and at the $E_{1/2}$ of the Prussian blue, $Fe_4(III)[Fe(II)(CN)_6]_3$ (0.2 V vs. Ag|AgCl in sat. KCl). An Ag|AgCl in saturated KCl and platinum wire were used as reference and counter electrodes, respectively. A bench top pH / ISE ORION meter, model 420A, was used for pH measurements. All solutions were

de-aerated by bubbling nitrogen prior to each electrochemical experiment. All experiments were performed at 25 ± 1 °C.

2.2.1 Preparation of the dopamine hydrochloride injection solution

A 2 mL (i.e, 80 mg) of the drug (dopamine hydrochloride injection- Dopamine HCl-Fresenius®) sample was diluted to 100 mL with de-ionised water. A 2 mL volume of the diluted solution was pipetted into individual 50 mL volumetric flasks and all except one were spiked with different concentration of standard dopamine solution, and made up to volume with phosphate buffer pH 7.0. The concentration of each test aliquot solution was determined using square wave voltammetry. Four different injections from the same batch were analysed using the same procedure. The experiment was repeated 5 times for each sample.

2.3 Electrode modification via sequential chemical deposition

The EPPGE surface was cleaned by gentle polishing in an aqueous slurry of alumina nanopowder, Sigma-Aldrich (grain size <100 nm) on a SiC-emery paper and finally to a mirror finish on a Buehler felt pad. The electrode was then subjected to ultrasonic vibration in absolute ethanol to remove residual alumina particles that might be trapped at the surface. EPPGE-SWCNTPABS was prepared by a drop-dry method. About 10 µL drop of the SWCNTPABS/H_2O solution (0.1 mg SWCNTPABS) in 1 ml H_2O) was added

drop-wise on the bare EPPGE and dried in an oven at 50 ^{o}C for about 2 min. The deposition of PB nanoparticles on the SWCNTPABS modified electrodes was carried out using a modified procedure by Han et al. [17]. Ferric chloride ($FeCl_3$) and $K_4[Fe(CN)_6]$ of the same concentration (10^{-4} M) were used for the deposition experiment. The EPPGE-SWCNTPABS electrode was immersed in $FeCl_3$ solution for 30 min, under stirring. Thereafter, the electrode was rinsed, dried and immersed in potassium ferrocyanide ($K_4[Fe(CN)_6]$) for another 30 min. It was then rinsed and dried to give the first layer of PB nanoparticles corresponding to the first deposition cycle, denoted here as EPPGE-SWCNT-PB. The second layer (EPPGE-SWCNT-2PB) and the third layer (EPPGE-SWCNT-3PB) of PB nanoparticles were obtained by repeating the procedure already described. The electrode formed in the absence of SWCNTPABS is denoted as EPPGE-PB.

3.0. Results and Discussion

3.1 AFM images, EDX and UV-vis spectra

Figure 1 shows the typical topographic AFM images of (a) bare glassy carbon (GC) plate, (b) GC-SWCNT-PABS and (c) GC-SWCNT-PB, and their corresponding 3D images and cross sectional profile. GC plate was used as substitute for EPPGE in obtaining characterisation data since it was the next available carbon based material that fitted conveniently into the AFM equipment. The GC plate (Fig. 1a) was predominantly carbon particles, but

was evenly covered by the carbon nanotubes arrays (Fig. 1b) after drop-dried. Successful deposition of PB nano particles on the GC plate was clearly indicated with the changes in the topography from Figure 1b to 1c. The topographic image of the GC-SWCNT-PB gave a particle size dimension in the nano range of about 10-90 nm (Fig. 1a) while the cross-sectional size diameter was about 5-15 nm compared to the bare-GC and the GC-SWCNTPABS with particle size diameters of about 2 and 10 nm respectively, indicating successful deposition of PB nanoparticles. The value agreed with 5-15 nm size distribution obtained from the transmission electron microscope image previously reported [39].

Figure 1 here

Figure 2 shows the EDX spectra for the bare GC (a), GC-SWCNTPABS (b) and the GC-SWCNT-PB (c) modified plates. The bare-GC and the GC-SWCNTPABS plates were predominantly occupied by carbon particles as indicated by the very pronounced and intense peak of carbon from their EDX spectra. The appearance of Fe peak in the GC-SWCNT-PB spectrum suggests that the electrode was successfully modified with PB nanoparticles ($Fe_4(III)[Fe(II)(CN)_6]_3$). The Fe peak can be attributed to the Fe^{3+} or Fe^{2+} ion of PB.

Figure 2 here

3.2. UV-vis-absorption spectroscopy characterization of the SWCNT-PABS, PB and the SWCNT-PB nanoparticles.

UV-vis absorption spectroscopic analyses were performed to further confirm the formation of the SWCNT-PB nanocomposite. Figure 3 compares the UV-vis spectra of the PB, SWCNTPABS and the SWCNT-PB solutions. The PB forms a stable nano films with the SWCNT-PABS through both π-π and electrovalent interactions [35,36]. The SWCNTPABS have a characteristic absorption band at about 243 nm which is lower than the 260 nm reported by Wang et. al. [44], and was described previously by authors as the characteristic of the adsorption of the assembled CNTs [45]. The difference can be attributed to the smooth and pure nature of the SWCNTPABS, with the absence of other light absorbing groups that may lead to an increased absorption band. The PB has a characteristic absorption band at approximately 667 nm, corresponding to the mixed-valence charge-transfer absorbance of the [Fe(II)-C-N-Fe(III)] complex. This result agreed with reported literature values [17,44]. The absorption bands at 243 nm for the SWCNTPABS disappeared after the deposition of PB nanoparticles on the SWCNTPABS to give SWCNT-PB nanoparticles, and a reduction in the PB band intensity indicating successful transformation of the SWCNTPABS to SWCNT-PB. Other spectroscopic techniques confirming the successful deposition of PB nanoparticles on the SWCNT-PABS were previously reported [39].

Figure 3 here

3.3. Electrocatalytic oxidation of dopamine

The stability of the film and the electrochemical characterisation of the fabricated electrodes EPPGE, EPPGE-PB, EPPGE-SWCNTPABS, EPPGE-CTABSWCNT-PB and EPPGE-SWCNT-PB used in this study were previously reported [39]. The corresponding electrochemical (cyclic voltammograms) responses of 2 x 10^{-4} M DA in PBS of pH 7.0 are shown in Figure 4a(i)-(v) for (i) bare EPPGE, (ii) EPPGE-SWCNTPABS, (iii) EPPGE-PB, (iv) EPPGE-SWCNT-PB and (v) EPPGE-CTABSWCNT-PB) respectively. After background current subtraction, the current density follows the order: EPPGE-SWCNT-PB (~ 617.0 μAcm^{-2}) > EPPGE-SWCNTPABS (~ 301.0 μAcm^{-2}) > bare-EPPGE (~ 124.0 μAcm^{-2}) > EPPGE-PB (~ 140.0 μAcm^{-2}). The trend shows that the best DA electrochemical response, in terms of current density was obtained at EPPGE-SWCNT-PB, in addition, it also exhibited the onset potential (~0.04 V). Similar experiment was performed using CTAB/SWCNT-PB electrodes where CTAB acts as PB stabilizer on the electrode. The result shows that CTAB modified electrodes gave poor DA response compared to electrode without CTAB (Fig. 4a), this is most likely due to the electrostatic repulsion between the CTAB cations and the positively DA molecules. Based on the result obtained, all subsequent studies were carried out with EPPGE-SWCNT-PB unless otherwise stated.

Figure 4 here

The impact of the number of PB layers on the electro-oxidation of DA using 0.1 mM deposition solution was then investigated. The result shows current response (after background subtraction) increase as the layer increased from one to three [295.0 μAcm^{-2} (SWCNT-3PB) (Fig. 4biii) > 257.0 μA (SWCNT-2PB) (Fig. 4bii) > 146.0 μAcm^{-2} (SWCNT-PB) (Fig. 4bi)]. Further increase in the number of PB layers shows no significant increase in the current density; an indication that further addition of PB might be forming a passive layer instead. Noteworthy, the same investigation carried out using higher concentrations of deposition solutions (1.0 and 10.0 mM) shows no significant increase in the current density. This is an indication that deposition solution concentration might not be playing a significant role in the rate or quantity of PB deposition rather; it is the deposition time. This outcome is not surprising since all the depositions were carried out using the same deposition time. Han et al. [17] also reported a similar observation and concluded that the low concentration of the deposition solution of PB is essential. Therefore, it would seem very reasonable and economical to use low concentrations (0.1 mM) of $FeCl_3$ and $K_4[Fe(CN)_6]$ for typical electrode modification with PB nanoparticles.

The electron transfer behaviour of the three electrodes (EPPEGE-SWCNT-PB, EPPGE-SWCNT-2PB and EPPGE-SWCNT-3PB) towards the oxidation of DA was studied by performing electrochemical impedance spectroscopy (EIS) experiments in 2×10^{-4} M DA solution at a fixed potential

of 0.2 V vs. Ag|AgCl, sat'd KCl. Figure 5a presents the Nyquist plots obtained and Figure 5b is the circuit used to fit the spectra. In the circuit, R_s represents the solution/electrolyte resistance, R_{ct} is the charge-transfer resistance, Z_w is the Warburg impedance related to the semi-infinite linear diffusion. EPPGE-SWCNT-3PB electrode has the fastest electron transport. The R_{ct} values followed the order: EPPGE-SWCNT-3PB (3.95 Ωcm^2) < EPPGE-SWCNT-2PB (5.01 Ωcm^2) < EPPGE-SWCNT-PB (5.33 Ωcm^2), indicating faster electron transfer towards DA electrocatalysis at the EPPGE-SWCNT-3PB.

Figure 5 here

Bode plot of –phase angle vs. log (*f*/Hz) obtained for the different PB layers (Figure 5c) gave phase angle values less than -90^o expected for ideal capacitive behaviour. Also, the *n* values obtained were less than 1.0, indicating the pseudocapacitive nature of the electrodes at every PB layer. Presently, there is little information on the electrochemical impedance study on DA oxidation.

3.4. Effect of varying scan rate

The effect of scan rate (25 to 1000 mVs^{-1}) on the EPPGE-SWCNT-3PB electrode kinetics during dopamine oxidation was investigated using cyclic voltammetry experiments. This procedure was repeated six times and the relative standard deviation (SD) obtained was <5%. A pair of well-defined redox peaks, with equal peak current heights at all scan rates, were observed

(Fig. 6a). The peak-to-peak separation (ΔE_p) increased from 76 mV at 25 mVs^{-1} to 654 mV at 1000 mVs^{-1}. Deviation of ΔE_p from the ideal 59.8 mV value expected for a one-electron reversible process is indicative of weak electron transfer as the scan rate increases. The plot of the anodic (I_{pa}) peak current against the square root of scan rate ($\nu^{1/2}$) is linear (Fig. 6b), with a negative intercept suggesting that the reaction at the electrode is not completely diffusion controlled but involves the adsorption of DA oxidation intermediates on the electrode surface. Using the Tafel equation (Eqn. 1) for a reversible process [46], and from the slope of the plot of peak potential (E_p) vs. $\log \nu$ for both the forward and the reverse processes (not shown), a Tafel slope of 558.6 $mVdec^{-1}$ was obtained which implied a strong binding of reactants or intermediates on the electrode surface, or reactions occurring within a porous electrode structure [47].

$$E_p = \frac{b}{2}\log \nu + const. \quad (1)$$

$$b = \frac{2.303RT}{\alpha n_\alpha F} \quad (2)$$

Figure 6 here

Furthermore, the catalytic reaction kinetics using the rotating disc electrode (RDE) technique was explored. This procedure was also repeated six times and the relative standard deviation (SD) obtained was <4%. Figure 6c depicts the RDE voltammograms obtained at different rotating speeds (ω) for

2 x 10^{-4} M DA electro-oxidation in PBS pH 7.0 using solution containing 2 x 10^{-4} M DA at the EPPGE-SWCNT-3PB. Figure 6d is the plot of I_{lim}^{-1} versus $\omega^{-1/2}$ employing the Koutecky-Levich Equation (Eq 3):

$$\frac{1}{i_{\lim}} = \frac{1}{i_k} + \frac{1}{i_{lev}} = \frac{1}{(nFAk_{ch}\Gamma C)} + \frac{1}{(0.620nFAcD^{2/3}\gamma^{-1/6}\omega^{1/2})} \quad (3)$$

where i_{lim}, i_k, i_{lev} are the measured current, kinetic and diffusion-limited currents, respectively, n is the number of electrons transferred which is 2 for DA electro-oxidation, k_{ch} is the catalytic rate constant ($mol^{-1}cm^3\ s^{-1}$), F is the Faraday constant (96485 C mol^{-1}), A is the electrode surface area (0.196 cm^2), ω is the rotating speed (rpm), Γ ($molcm^{-2}$) is the redox active species (4.78 x 10^{-8} mol cm^{-2}) concentration on electrode surface, c is the bulk concentration of DA (2 x 10^{-7} $molcm^{-3}$), D is the diffusion coefficient (cm^2s^{-1}) of DA and γ is the kinematic viscosity of the solution. The plot obtained was linear with a positive intercept, indicating that the electrode reactions were controlled by both kinetics at the electrode surface and the mass transport of DA species. The k_{ch} value obtained from the intercepts of the regression lines was found to be 1.69 x 10^5 $mol^{-1}cm^3s^{-1}$ (1.69 x 10^2 M^{-1} s^{-1}) which agreed closely with the range of 3.3 x 10^2 to 2.9 x 10^2 M^{-1} s^{-1} for the DA concentration range (5 - 7.5 mM), reported for aluminium electrode modified with nickel pentacyanonitrosylferrate films (NiPCNF/Al) [48]. The difference in the k_{ch} value is due to the catalytic interaction of DA with the different electrode modifiers. In correcting the polarization curve for diffusion effects for first

order reactions, the Tafel equation may be simplified as shown in Equation 4 [46,49,50]:

$$E_{app} = E_{eq} + \frac{b}{2}\log I_K \quad (4)$$

$$I_K = \frac{(i_L . i)}{(i_L - i)} \quad (5)$$

where E_{app} is the applied potential, E_{eq} is the equilibrium potential, I_k is the kinetic current, i_L is the limiting current (plateau in RDE voltammogram), i is the measured current at a given potential, R, T and F have their usual meanings, αn is the kinetic parameters for the electrode process. At 2500 rpm, the plot of E_{app} versus log I_k (inset in Fig. 6d) a Tafel slope of 112 $mVdec^{-1}$ was obtained which further confirmed the adsorption process already reported under scan rate study. The difference in the Tafel values may be due to the sensitive nature and the fast kinetics at RDE electrode compared to CV experiment. Based on the results, the following reaction mechanism (scheme 1.0) may be proposed for the electrocatalytic oxidation of DA at the EPPGE-SWCNT-3PB:

$$SWCNT\text{-}PAB\text{-}SO_3^{2-}/Fe^{3+}/Fe^{2+} \longrightarrow SWCNT\text{-}PAB\text{-}SO_3^{2-}/Fe^{3+}/Fe^{3+} + e^- \quad (6)$$

$$SWCNT\text{-}PAB\text{-}SO_3^{2-}/Fe^{3+}/Fe^{3+} + DA^+ \longrightarrow SWCNT\text{-}PAB\text{-}SO_3^{2-}/Fe^{3+}/Fe^{3+}\text{-----}DA^+ \quad (7)$$

$$SWCNT\text{-}PAB\text{-}SO_3^{2-}/Fe^{3+}/Fe^{3+}\text{-----}DA^+ \longrightarrow SWCNT\text{-}PAB\text{-}SO_3^{2-}/Fe^{3+}/Fe^{2+} + QDA^+ + 2H^+ + e^- \quad (8)$$

Slow (rate determining step)

$$SWCNT\text{-}PAB\text{-}SO_3^{2-}/Fe^{3+}/Fe^{3+} + e^- \longrightarrow SWCNT\text{-}PAB\text{-}SO_3^{2-}/Fe^{3+}/Fe^{2+} \quad (9)$$

Scheme 1: Proposed mechanism for the electrocatalytic oxidation of DA on EPPGE-SWCNT-PB modified electrode.

At pH 7, DA (p*Ka* 8.9) exists as a cation with a positively charged amino group [51]. Equation (6) represents the catalyst redox pre-equilibrium reaction which shows the electrochemically driven oxidation of the Fe^{2+} ions in SWCNTPAB-$SO_3^{2-}/Fe^{3+/}Fe^{2+}$ to SWCNTPAB-$SO_3^{2-}/Fe^{3+/}Fe^{3+}$. Thereafter, the oxidised catalyst form adduct with DA (Eqn 7) where oxidation of DA to dopamine-O-quinone (QDA^+) through a two-electron oxidation process and simultaneously, reduction of the oxidised catalyst to the original form takes place. This represents the rate (slow) determining step (rds) (Eqn 8). The catalyst is regenerated by the reduction process as represented in Equation 9.

3.5. Electroanalysis using square wave voltammetry (SWV), chronoamperometric (CA) and linear sweep voltammetry (LSV).

Concentration studies were carried out using different techniques at a fixed potential of 0.20 V. This procedure was repeated five times and the relative standard deviation (SD) obtained was <3%. These are exemplified by chronoamperometry (Fig 7a) and linear sweep voltammograms (Fig 7b).

Figure 7 here

From the plots of current response against concentration, linear relationships (Equations 10-13) were obtained as follows:

CA: I_p / μA=(116.01±1.58) [DA] / μM + (0.82±0.10) (R^2 = 0.9994) (10)

CA: I_p / μA = (7.94±0.16) [DA] / μM + (11.66±0.11) (R^2 = 0.9992) (11)

SWV: I_p / μA = (4.82±0.05) [DA] / μM + (169.40±0.68) (R^2 = 0.9992) (12)

LSV: I_p / μA = (0.65±0.07) [DA] / μM + (27.78±0.39) (R^2 = 0.9993) (13)

The limit of detections for the different techniques employed in this study were calculated using (LoD = 3.3 s/m [52]) (where *s* is the relative standard deviation of the intercept and *m* is the slope of the linear current versus concentration of DA) and the linear concentration range were also determined. The LoD values are 2.8 nM and 0.4 x 10^{-8} M at concentration range of 0.01 – 0.1 and 0.1 – 1.0 μM using chronoamperometric technique. The analytical data obtained in this study compared favourably and even

better with other values earlier reported in the literature for some modified electrodes towards DA detection [53-59]. The LoD value (2.7 nM) was about order of 2 magnitudes better compared to the value obtained from our recent work with Fe_2O_3 nanoparticle modified electrode [53].

The re-usability and stability of the EPPGE-SWCNT-3PB were also examined. The electrode was firstly repeatedly cycled (50 runs) in pH 7.0 PBS containing 2 x 10^{-4} M DA (not shown). The current decreased from the first scan until about the 30^{th} scan where it stabilised. The initial current drop from continuous recycling without rinsing before the next run is not surprising; freshly prepared electrodes often need to stabilise in the immersed solution, also initial adsorption of the DA oxidation product intermediates cannot be ruled out. However, upon rinsing the electrode in a fresh electrolyte solution and the analysis repeated, about 85% of the initial current height of the DA was obtained, suggesting the electrode can be reused after analysis. Similarly, after storage for two weeks in a refrigerator, no significant change in DA current was observed which confirmed the electrode stability towards the analyte.

3.6. Detection of DA in the presence of AA (Interference study)

Figure 8a is the cyclic voltammetric responses of EPPGE-SWCNT-3PB electrode in (i) 0.1 M pH 7.0 PBS, (ii) 10 mM AA alone, and mixture of (iii) 9.1 µM DA and 9.1 mM AA, (iv) 16.7 µM DA and 8.3 mM AA, (v) 23.1 µM DA and

7.7 mM AA, (vi) 28.6 μM DA and 7.1 mM AA, (vii) 33.3 μM DA and 6.7 mM AA and (viii) 41.2 μM DA and 5.9 mM AA in PBS pH 7.0. The AA signal which was initially observed at around 0.0 V in the absence of DA remained the same after addition of DA, while the DA signal occurred at around 0.2 V. It is worth noting that DA could be simultaneously detected even at high AA concentration (9.1 mM), which was 1000 times more than that of DA (9.1 μM), and a potential separation of about 200 mV. The height and amplitude of the peak corresponding to DA also increased proportionally with the DA concentration. This is a strong indication that for all the concentrations of the DA studied there was no detectable interference of AA. On the other hand, at the bare EPPGE (Fig. 8b), AA peaks completely interfered and suppressed the DA signal at around 0.2 V. Indeed, this result is unique and presents a better DA/AA separation signals when compared to a recent work with Fe_2O_3 nano particle for the simultaneous detection of DA and AA [53].

Figure 8 here

3.7. *Real sample analysis: Dopamine drug*

To evaluate the potential applicability of the EPPGE-SWCNT-3PB electrode, a square wave voltammetric assay of dopamine present in a dopamine hydrochloride injection, with dopamine content of 200 mg / 5 mL (i.e. 40 mg mL^{-1}) was carried out. The concentration found in each dopamine drug was approximately within the range of the labelled amount, with an

average recovery (n=5) of 101.60±2.79% at 95% confidence limit. This result further confirmed the suitability and reliability of the EPPGE-SWCNT-3PB electrode as a potential sensor for the analysis of neurotransmitters such as DA.

4.0 Conclusion

This study investigated the electron transfer behaviour and the catalysis of EPPGE modified with and without SWCNT-PABS/PB nanoparticles towards DA oxidation. The catalysis of DA was more favoured on the EPPGE-SWCNT-PB electrode in terms of current response and onset potential for catalysis compared to other electrodes investigated. DA response increased with increasing PB layer on the electrode making EPPGE-SWCNT-3PB the best electrode. The EPPGE-SWCNT-3PB electrode exhibited the fastest electron transport property and the lowest R_{ct} towards DA electrocatalysis. The electrode could conveniently detect DA in the presence of AA (1000 times higher) with a wide potential separation of about 200 mV. The electrode was found to be electrochemically stable, re-usable and can thus be used for the analysis of DA in real drug samples with satisfactory accuracy and reproducibility.

Acknowledgement

We thank the University of Pretoria and the National Research Foundation (NRF, GUN # 2073666). A.S.A thanks Obafemi Awolowo University, Nigeria for the study leave and University of Johannesburg for the post-doctoral research fellow.

References

[1] Z. H. Guo, S. J. Dong, Anal. Chem. 76 (2004) 2683.

[2] C. E. Banks, R. G. Compton, Analyst 131 (2006) 15.

[3] Z. W. Pan, S. S. Xie, L. Lu, B. H. Chang, L. F. Sun, W. Y. Zhou, G. Wang, D. L. Zhang, Appl. Phys. Lett. 74 (1999) 3152.

[4] B. O. Agboola, K. I. Ozoemena, T. Nyokong, T. Fukuda, N. Kobayashi, Carbon 48 (2010) 763.

[5] R. P. Deo, N. S. Lawrence, J. Wang, Analyst 129 (2004) 1076.

[6] B. O. Agboola, S. L. Vilakazi, K. I. Ozoemena, J. Solid State Electrochem. 13 (2009) 1367.

[7] Y. Zhao, Y. Gao, D. Zhan, H. Liu, Q. Zhao, Y. Kou, Y. Shao, M. Li, Q. Zhuang, Z. Zhu, Talanta 66 (2005) 51.

[8] A. Salimi, C. E. Banks, R. G. Compton, Analyst 129 (2004) 225.

[9] A. S. Adekunle, K. I. Ozoemena, J. Solid State Electrochem. 12 (2008) 1325.

[10] R. R. Moore, C. E. Banks, R. G. Compton, Analyst 129 (2004) 755.

[11] N. Maleki, A. Safavi, F. Tajabadi, Anal. Chem. 78 (2006) 3820.

[12] D. Nkosi, K. I. Ozoemena, J. Electroanal. Chem. 621 (2008) 304.

[13] D. Nkosi, K. I. Ozoemena, Electrochim. Acta 53 (2008) 2782.

[14] J. Pillay, B.O. Agboola, K. I. Ozoemena, Electrochem. Commun. 11 (2009) 1292.

[15] J. J. Gooding, Electrochim. Acta 50 (2005) 3049.

[16] Z. Song, J. Huang, B. Wu, H. Shi, J. Anzai, Q. Chen, Sens. Actuat. B 115 (2006) 626.

[17] S. Han, Y. Chen, R. Pang, P. Wan, M. Fan, Ind. Eng. Chem. Res. 46 (2007) 6847.

[18] L. Gorton, Electroanalysis 7 (1995) 23.

[19] Y. Shan, G. Yang, J. Gong, X. Zhang, L. Zhu, L. Qu, Electrochim. Acta 53 (2008) 7751.

[20] P. R. Somani, S. Radhakrishnan, Mater. Chem. Phys. 77 (2003) 117.

[21] A.V. Borisova, E.E. Karyakina, S. Cosnier, A.A. Karyakin, Electroanalysis 21 (2009) 409.

[22] D. M. DeLongchamp, P.T. Hammond, Adv. Funct. Mater. 14 (2004) 224.

[23] M. Pyrasch, A. Toutianoush, W.Q. Jin, J. Schnepf, B. Tieke, Chem.Mater. 15 (2003) 245.

[24] L. Zhang, Z. Song, Q. Zhang, X. Jia, H. Zhang, S. Xin, Electroanalysis 21 (2009) 1835.

[25] M. Jayalakshimi, F. Scholz, J. Power Sources 87 (2000) 212.

[26] S. J. Nakanishi, G. T. Lu, H. M. Kothari, E. W. Bohannan, J. A. Switzer, J. Am. Chem. Soc. 125 (2003) 14998.

[27] Marcin Karbarz, Marianna Gniadek, Zbigniew Stojek, Electroanalysis 21 (2009) 1363.

[28] S. Vaucher, M. Li, S. Mann, Angew. Chem. Int. Ed. 39 (2000) 1793.

[29] N. Bagkar, R. Ganguly, S. Choudhury, P. A. Hassan, S. Sawanta, J. V. Yakhmi, J. Mater. Chem. 14 (2004) 1430.

[30] J. M. Dominguez-Vera and E. Colacio, Inorg. Chem. 42 (2003) 6983.

[31] M. Yamada, M. Arai, M. Kurihara, M. Sakamoto, M. Miyake, J. Am. Chem. Soc. 126 (2004) 9482.

[32] W. Kosaka, M. Tozawa, K. Hashimoto, S.-I. Ohkoshi, Inorg. Chem. Commun. 9 (2006) 920.

[33] V. Vo, N. V. Minh, H. I. Lee, J. M. Kim, Y. Kim, S. J. Kim, Mater. Res. Bull. 44 (2008) 78.

[34] X. M. Wang, Z. Gershman, A. B. Kharitonov, E. Katz, I. Willner, Langmuir 19 (2003) 5413.

[35] Y. J. Zhang, Y. Wen, Y. Liu, J. H. Li, Electrochem. Commun. 6 (2004) 1180.

[36] Q. Lei, X. Y. Yang, Colld. Surf. A: Physicochem. Eng. Aspects, 278 (2006) 123.

[37] Y. Xian, Y. Zhoua, Y. Xian, L. Zhouc, H. Wang, L. Jin, Anal. Chimic Acta 546 (2005) 139.

[38] R. Bash, P. Thavarungkul, P. Kanatharana, J. Wang, Electroanalysis 20 (2008) 308.

[39] A.S. Adekunle, K.I. Ozoemena, Electroanalysis (21) 2010, 2519.

[40] W. Schultz, Curr.Opin. Neurobiol. 7 (1997) 191.

[41] S. Komathi, A. I. Gopalan, K.-P. Lee, Analyst 135 (2010) 397.

[42] J. W. Mo, B. Ogorevc, Anal.Chem. 73 (2001) 1196.

[43] R. M. Wightman, L. J. May, A. C. Michael, Anal. Chem. 60 (1998) 769A.

[44] L. Wang, S. Guo, X. Hu, S. Dong, Colld. Surf. A: Physicochem. Eng. Aspects 317 (2008) 394.

[45] Z. Xu, N. Gao, H. Chen, S. Dong, Langmuir 21 (2005) 10808.

[46] A. J. Bard, L. R. Faulkner, Electrochemical methods-fundamentals and applications 2001, Wiley, New York.

[47] J. N. Soderberg, A. C. Co, A. H. C. Sirk, V. I. Birss, J. Phys. Chem. B. 110 (2006) 10401.

[48] H. Razmi, M. Agazadeh, B. Habibi-A, J. Electroanal. Chem. 547 (2003) 25.

[49] N. Kobayashi, Y. Nishiyama, J. Phys. Chem. 89 (1985) 1167.

[50] N. Sehlotho, T. Nyokong, J. Electroanal. Chem. 595 (2006) 161.

[51] M. J. Giz, B. Duong, N. J. Tao, J. Electroanal. Chem. 465 (1999) 72.

[52] G. D. Christian, Analytical Chemistry, 6th ed. John Wiley and Sons New York, 2004, p113.

[53] A.S. Adekunle, B.O. Agboola, J. Pillay, K.I. Ozoemena, Sens. Actuat. B 148 (2010) 93.

[54] Z. Wang, J. Liu, Q. Liang, Y. Wang, G. Luo, Analyst 127 (2002) 653.

[55] D. Zheng, J. Ye, W. Zhang, Electroanalysis 20 (2008) 1811.

[56] S. Shahrokhian, H. R. Zare-Mehrjardi, Sens. Actuators B Chem. 121 (2007) 530.

[57] Y. Li, X. Lin, Sens. Actuators B Chem. 115 (2006) 134.

[58] A. Balamurugan, S. Chen, Bioelectrochem. 54 (2001) 169.

[59] G. Alarco´n-Angeles, B. Pe´rez-Lo´pez, M. Palomar-Pardave, M.T. Ramı´rez-Silva, S. Alegret, A. Merkoci, Carbon 46 (2008) 898.

[60] S. J. Richard Prabakar, S. Sriman Narayanan, Electroanalysis 21 (2009) 21, 1481.

Figure Captions and Tables

Figure 1: Typical topographic AFM images of (a) bare glassy carbon (GC) plate, (b) GC-SWCNTPABS and (c) GC-SWCNT-PB, and their corresponding 3D image and cross sectional profile.

Figure 2: EDX elemental profile of (a) bare GC plate (b) GC-SWCNTPABS and (c) GC-SWCNT-PB electrodes.

Figure 3: UV/VIS spectra of Prussian blue (PB), SWCNTPABS and SWCNT-PB.

Figure 4: Cyclic voltammograms showing the current responses of (a) (i) bare EPPGE, (ii) EPPGE-SWCNTPABS, (iii) EPPGE-PB, (iv) EPPGE-SWCNT-PB and (v) EPPGE-CTABSWCNT-PB in 0.1 M pH 7.0 PBS containing 2 $x10^{-4}$ M DA (scan rate: 25 mVs^{-1}). (b) (i) EPPGE-SWCNT-PB, (ii) EPPGE-SWCNT-2PB and (iii) EPPGE-SWCNT-3PB in 0.1 M pH 7.0 PBS containing 0.1 mM DA (after background current subtraction, scan rate: 25 mVs^{-1}).

Figure 5: (a) Typical Nyquist plots obtained for (i) EPPGE-SWCNT-PB, (ii) EPPGE-SWCNT-2PB and (iii) EPPGE-SWCNT-3PB in 0.1 M pH 7.0 PBS containing 2 $x10^{-4}$ M DA. The data points are experimental while the solid lines in the spectra represent non-linear least squares fits. (b) Circuit used in fitting the impedance data. (c) Bodes plot of –phase angle versus log *f*, and log $|Z/\Omega|$ versus log *f* for the electrodes in (a) above.

Figure 6: (a) Cyclic voltammogram showing the current response of EPPGE-SWCNT-3PB electrodes in 0.1 M PBS solution containing 2 x 10^{-4} M DA (scan rate: 25 to 1000 mVs^{-1}). (b) plot of I_p vs. $\nu^{1/2}$ (c) a RDE voltammograms

obtained for the EPPGE-SWCNT-3PB in 0.1 M PBS solution containing 2 x 10^{-4} M DA (rotating disc speed: 100 to 2900 rpm) (d) is the plot of I_p^{-1} vs. $\omega^{-1/2}$. Inset in (d) is the plot of E/V versus log [i x i_L/i_L – i].

Figure 7: (a) Chronoamperograms evolution of the EPPGE-SWCNT-3PB in 0.1 M PBS solution containing different concentrations of DA (0.0, 0.02, 0.05, 0.08, 0.1, 0.4, 0.8, 1.0 µM (inner to outer; i – xiii). Inset in (a) is the linear plot obtained from current versus DA concentration. (b) Linear sweep voltammogram responses of the EPPGE-SWCNT-3PB in 0.1 M PBS solution containing different concentrations of DA (0.00, 18.2, 28.6, 37.8, 50, 60.5, 66.7, 72.3 µM (inner to outer; i – viii).

Figure 8: Typical cyclic voltammograms responses of EPPGE-SWCNT-3PB in (i) 0.1 M pH 7.0 PBS, (ii) 10 mM AA alone, and mixture of (iii) 9.1 µM DA / 9.1 mM AA, (iv) 16.7 µM DA / 8.3 mM AA, (v) 23.1 µM DA / 7.7 mM AA, (vi) 28.6 µM DA/7.1 mM AA, (vii) 33.3 µM DA/6.7 mM AA and (viii) 41.2 µM DA/5.9 mM AA in PBS pH 7.0. (b) Square wave voltammograms of bare EPPGE in pH 7.0 PBS alone, 10 mM AA alone, and 10 mM AA + 2ml and 8 ml $1x10^{-4}$ M DA solutions respectively.

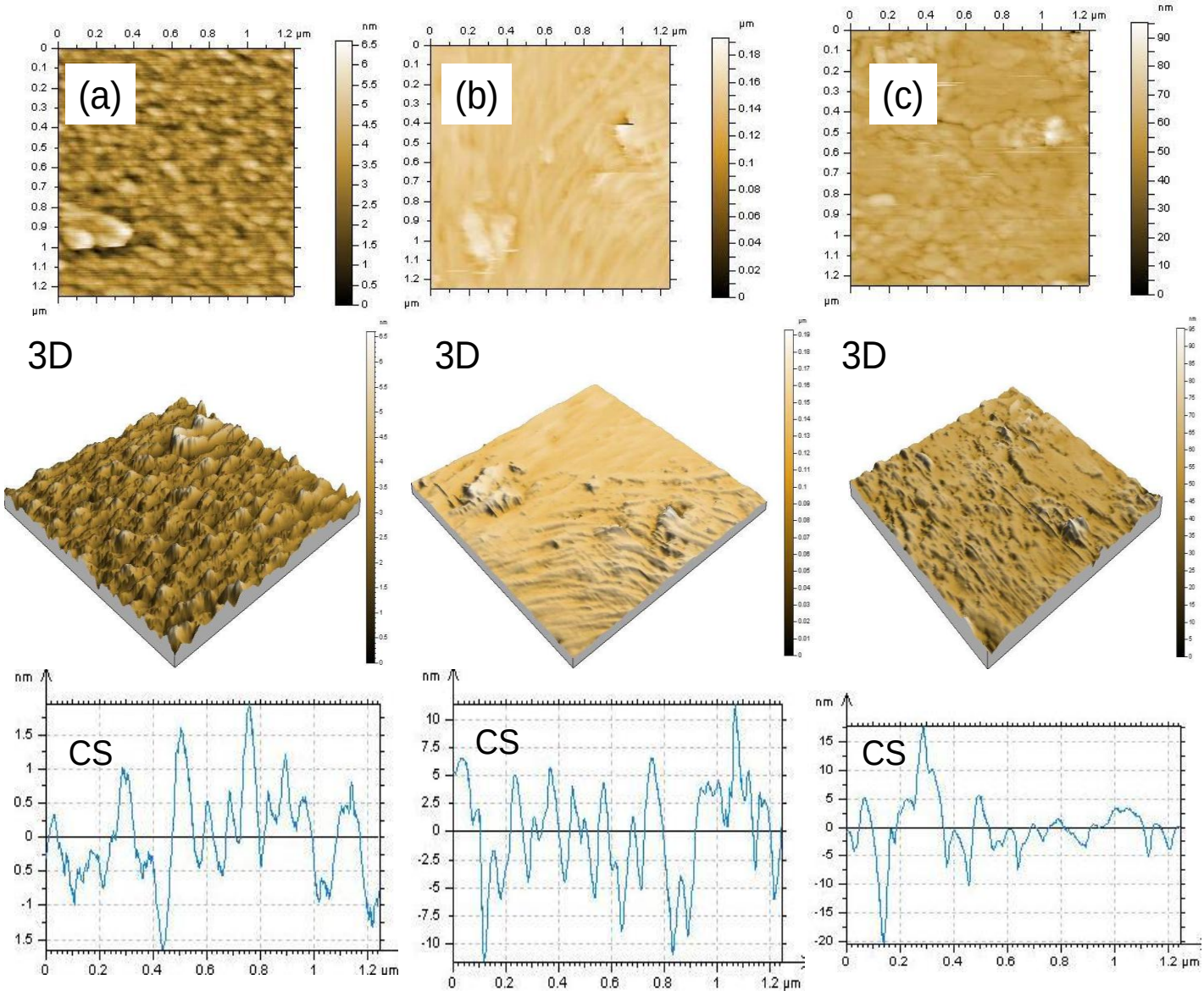

Figure 1

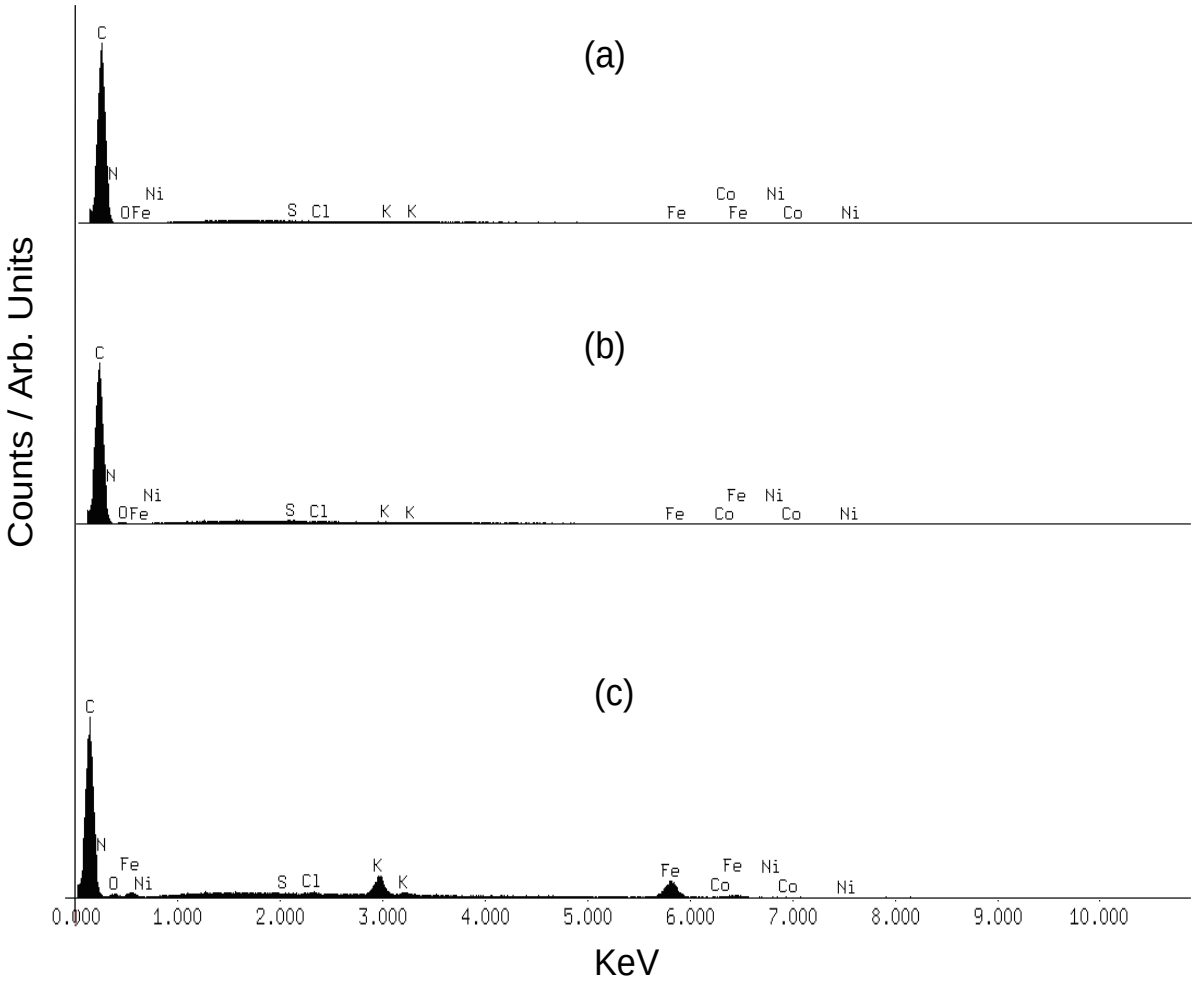
(a)
(b)
(c)
C
N
O
Fe
Ni
S
Cl
K
Co
Counts / Arb. Units
0.000
1.000
2.000
3.000
4.000
5.000
6.000
7.000
8.000
9.000
10.000
KeV

Figure 2

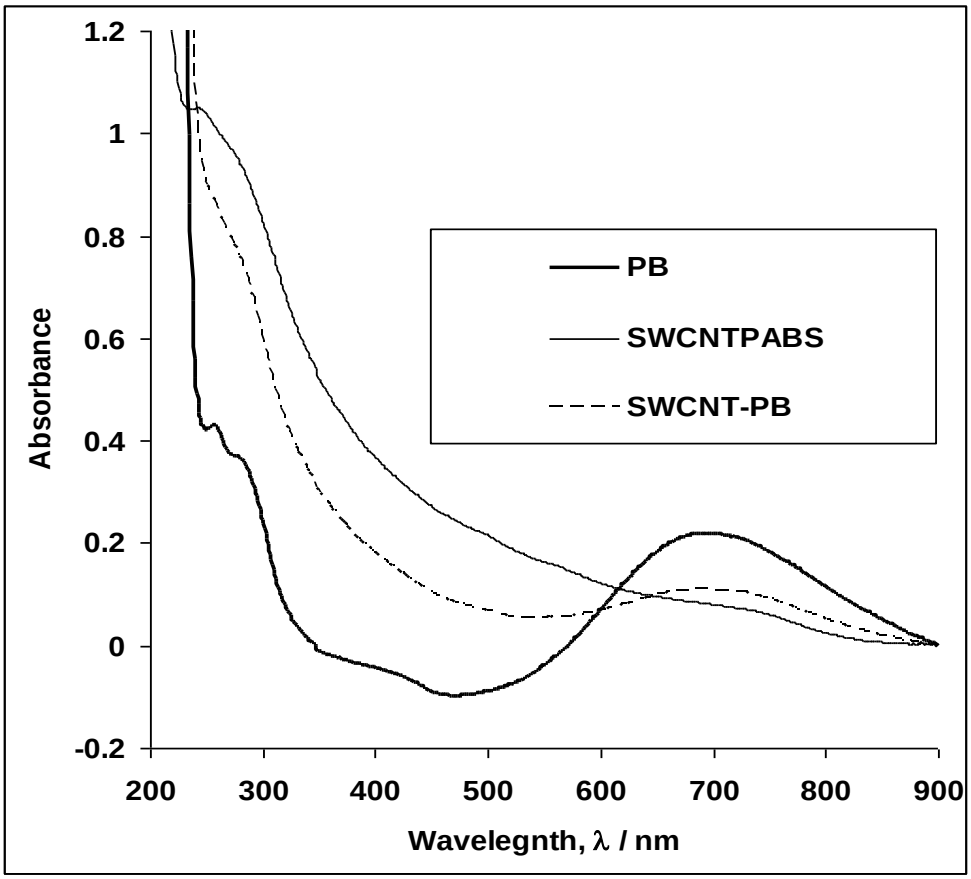
1.2
1
0.8
0.6
0.4
0.2
0
-0.2
Absorbance
200
300
400
500
600
700
800
900
Wavelegnth, λ / nm
PB
SWCNTPABS
SWCNT-PB

Figure 3

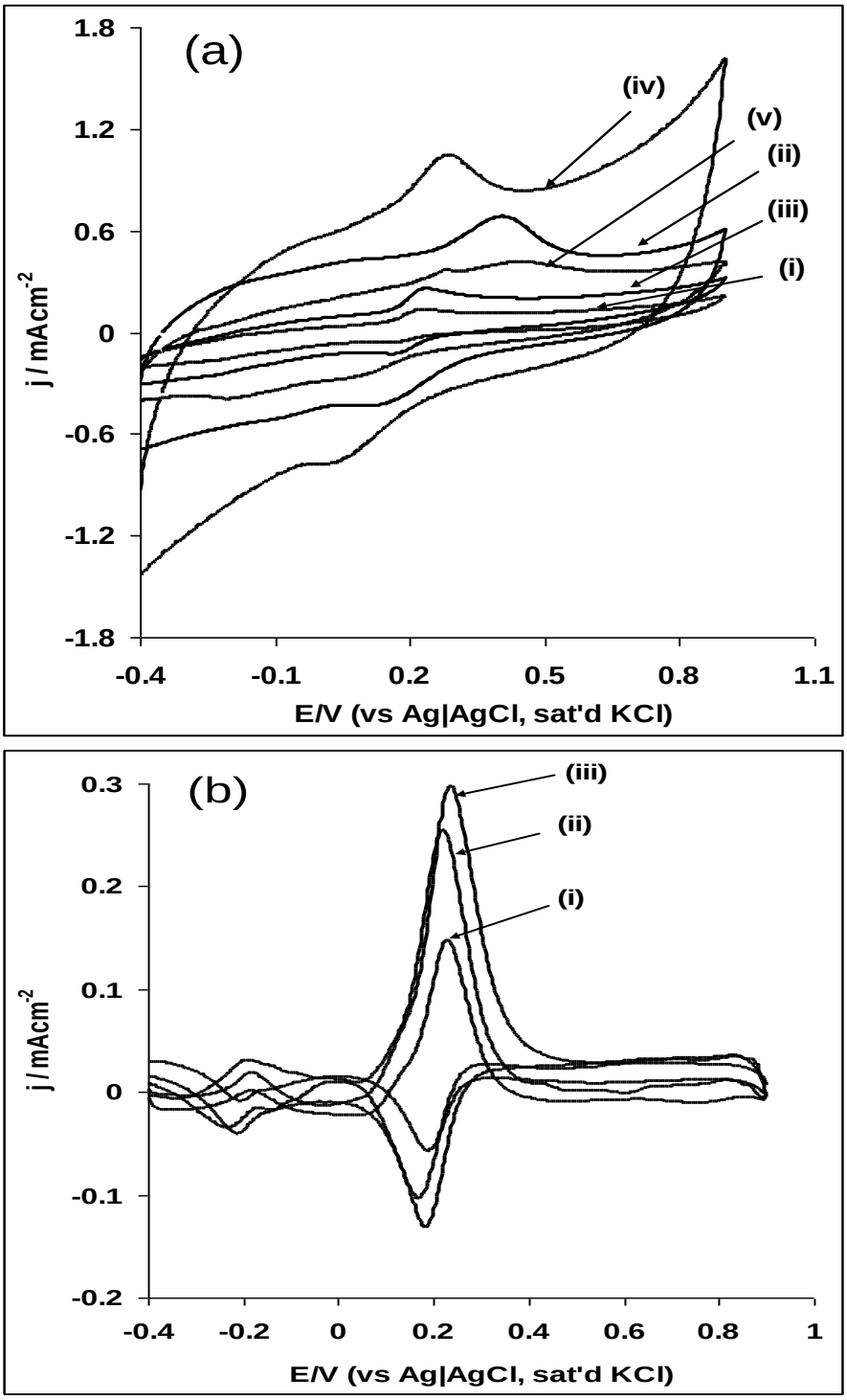
(a)
(iv)
(v)
(ii)
(iii)
(i)
1.8
1.2
0.6
0
-0.6
-1.2
-1.8
j / mAcm-2
-0.4
-0.1
0.2
0.5
0.8
1.1
E/V (vs Ag|AgCl, sat'd KCl)
(b)
(iii)
(ii)
(i)
0.3
0.2
0.1
0
-0.1
-0.2
j / mAcm-2
-0.4
-0.2
0
0.2
0.4
0.6
0.8
1
E/V (vs Ag|AgCl, sat'd KCl)

Figure 4

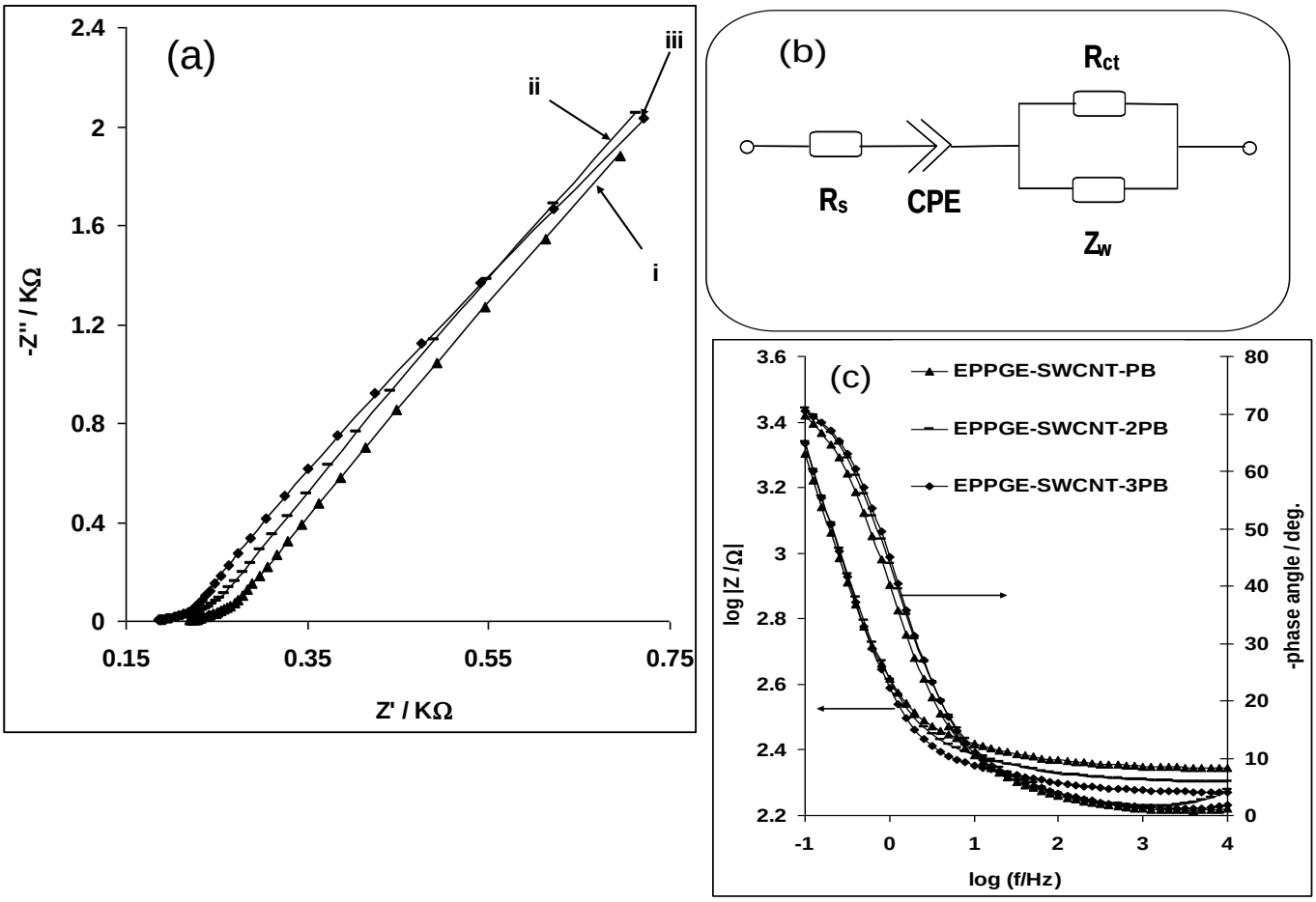
(a)
iii
ii
i
-Z'' / KΩ
Z' / KΩ
2.4
2
1.6
1.2
0.8
0.4
0
0.15
0.35
0.55
0.75
(b)
Rct
Rs
CPE
Zw
(c)
EPPGE-SWCNT-PB
EPPGE-SWCNT-2PB
EPPGE-SWCNT-3PB
log |Z /Ω|
-phase angle / deg.
log (f/Hz)
3.6
3.4
3.2
3
2.8
2.6
2.4
2.2
80
70
60
50
40
30
20
10
0
-1
0
1
2
3
4

Figure 5

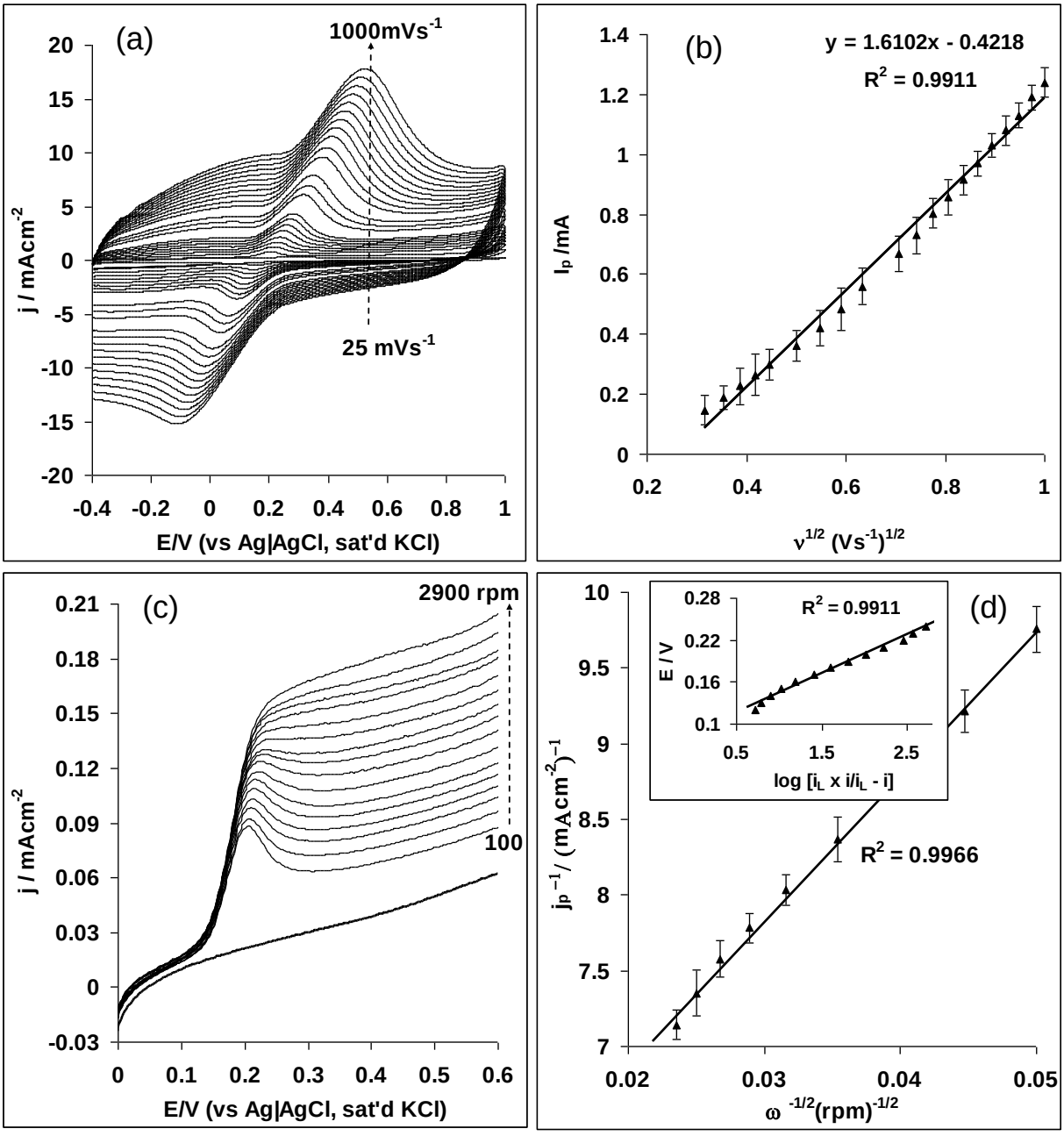
(a)
1000mVs-1
25 mVs-1
j / mAcm-2
E/V (vs Ag|AgCl, sat'd KCl)
(b)
y = 1.6102x - 0.4218
R2 = 0.9911
Ip /mA
ν1/2 (Vs-1)1/2
(c)
2900 rpm
100
j / mAcm-2
E/V (vs Ag|AgCl, sat'd KCl)
(d)
R2 = 0.9911
E / V
log [iL x i/iL - i]
R2 = 0.9966
jp-1/ (mAcm-2)-1
ω -1/2(rpm)-1/2

Figure 6

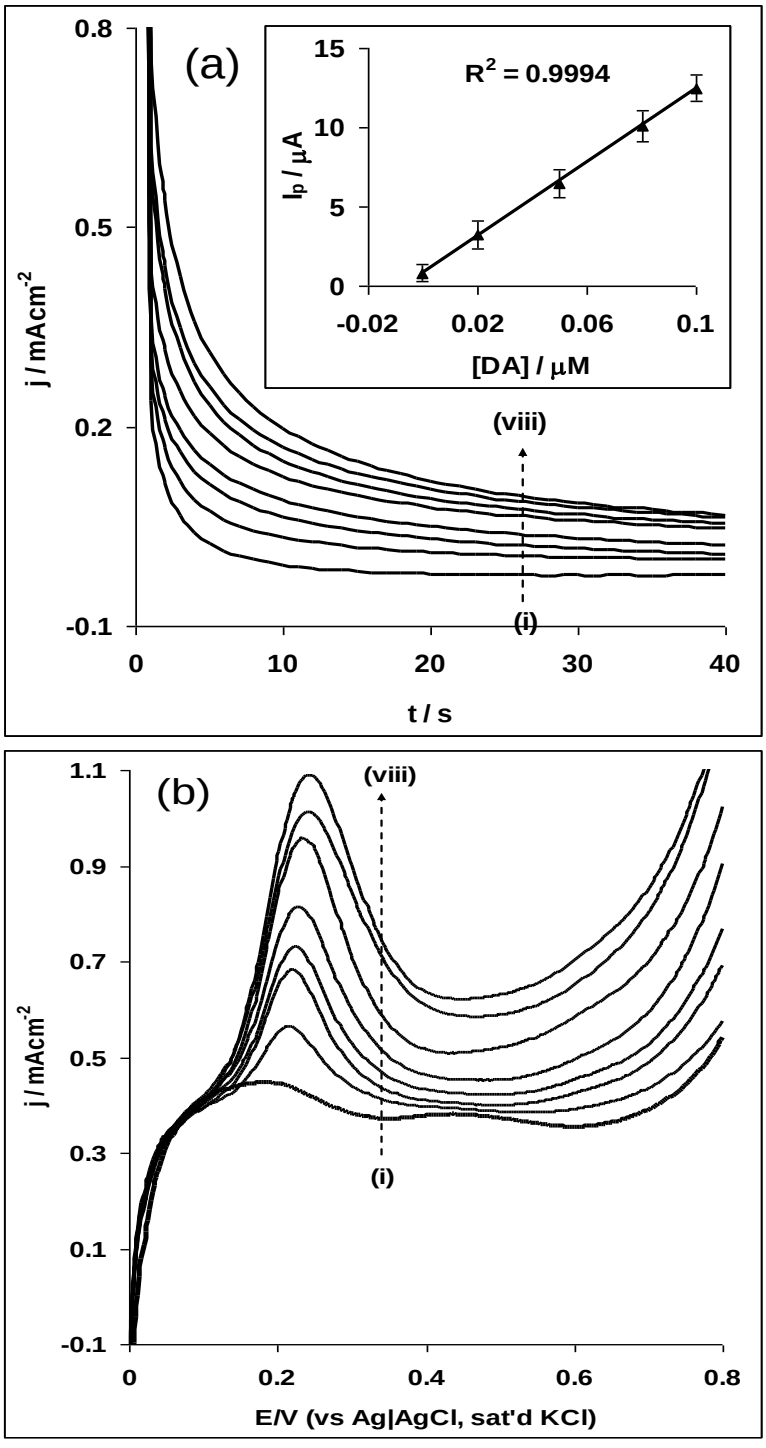
(a)
0.8
0.5
0.2
-0.1
j / mAcm-2
0
10
20
30
40
t / s
(viii)
(i)
15
10
5
0
Ip / μA
R2 = 0.9994
-0.02
0.02
0.06
0.1
[DA] / μM
(b)
1.1
0.9
0.7
0.5
0.3
0.1
-0.1
j / mAcm-2
0
0.2
0.4
0.6
0.8
E/V (vs Ag|AgCl, sat'd KCl)
(viii)
(i)

Figure 7

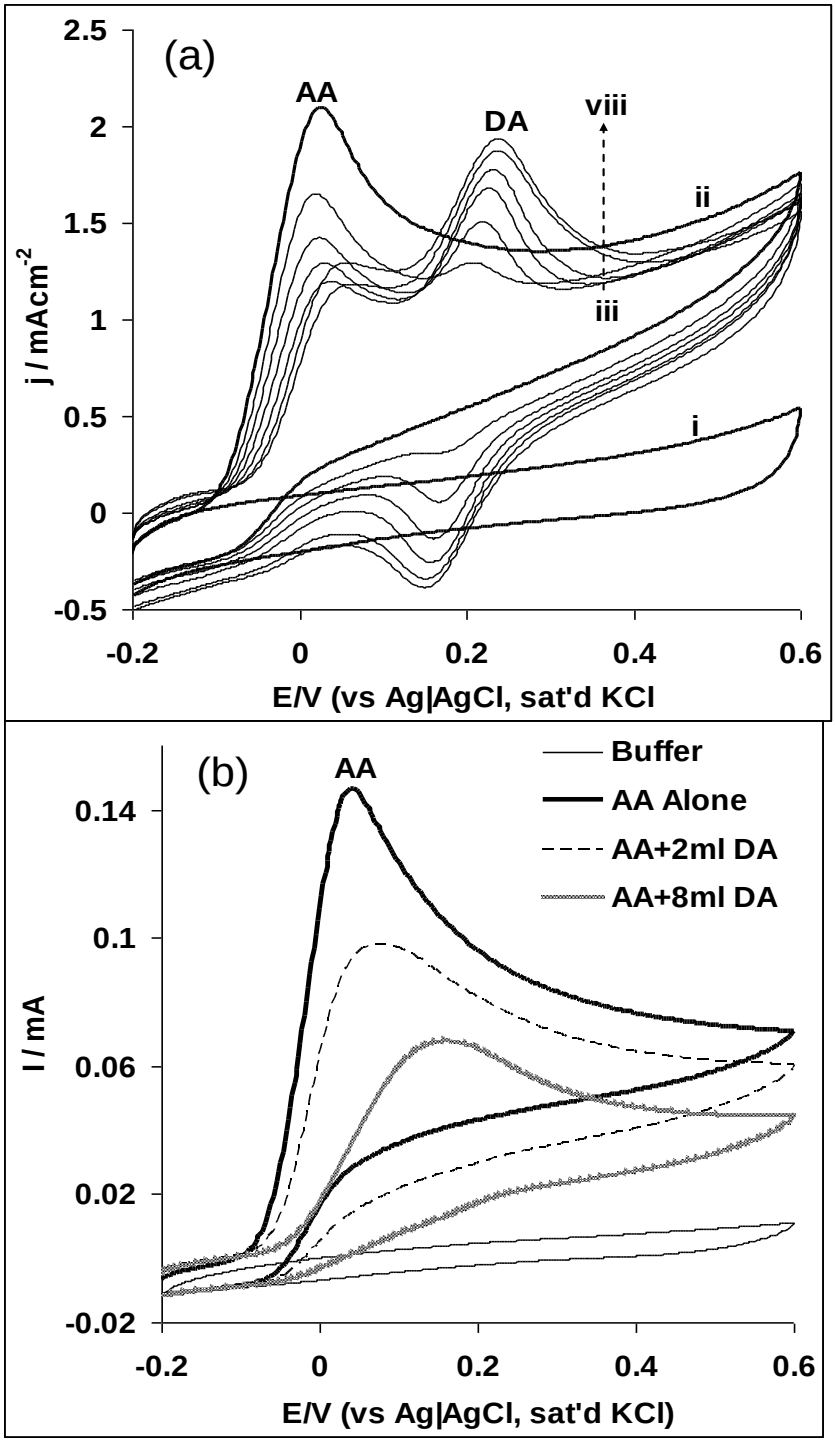
(a)
AA
DA
viii
ii
iii
i
2.5
2
1.5
1
0.5
0
-0.5
j / mAcm-2
-0.2
0
0.2
0.4
0.6
E/V (vs Ag|AgCl, sat'd KCl
(b)
AA
Buffer
AA Alone
AA+2ml DA
AA+8ml DA
0.14
0.1
0.06
0.02
-0.02
I / mA
-0.2
0
0.2
0.4
0.6
E/V (vs Ag|AgCl, sat'd KCl)

Figure 8